Simulation of adsorption and desorption of VOC on activated carbon

Sviatoslav Eroshkin[a], Eivind Johannessen[b], Even Solbraa[c]

[a, c] *Department of Energy and Process Engineering, Norwegian University of Science and Technology*
[b ,c] *Equinor*
eroshkin.sviatoslav @gmail.com

Abstract

The study's primary purpose is to simulate the adsorption and desorption of volatile organic components on activated carbon bed using python. The model was verified with experiments for the separation of methane (55 mol %) - carbon dioxide (45 mol %) mixture using vacuum pressure swing adsorption on an activated carbon molecular sieve. For a six-component mixture (methane, ethane, propane, butane, carbon dioxide and nitrogen), the model was verified using Aspen Adsorption flowsheet simulator and experimental results of vacuum pressure swing adsorption on activated carbon. Even though the model showed a relatively low error in comparison with provided experiments, some experimental cases need to be investigated more to get a better model prediction.

1. Introduction

Adsorption of VOC (Volatile Organic Components) on a fixed-bed AC (Activated Carbon) is commonly used to reduce VOC emissions. VRU (Vapor Recovery Units) gained popularity in the 1990s. Today 95 % of all new VRU are based on AC adsorption followed by vacuum regeneration.

Many papers have studied the PSA (Pressure Swing Adsorption) for other components than VOC. From the technical point of view, these works are interesting because the mechanism of VOC VPSA (Vacuum Pressure Swing Adsorption) is in many ways similar. The PSA process exploits the change of the adsorption equilibrium with a change in system pressure. The process efficiency depends on many factors such as the number, sequence, and time of PSA steps, flow rate of the gas, gas composition, adsorption pressure, and others. For example, Kim et al. (2015) investigated biogas mixture adsorption on AC molecular sieve with four beds and a seven steps PSA system. A significant improvement to the PSA process was the equalization step: reducing the energy consumption in the pressurization step by employing the purified product from the second adsorber. The experimental setup and numerical model showed a cyclic steady-state process after 13 cycles.

Furthermore, Kim et al. (2015) indicate that optimum conditions for the separation highly depend on such parameters as the adsorption pressure, desorption pressure, purge, and feed rates (the ratio of the purge gas flow rate to the flow rate of desirable component feed rate). Ahn et al. (2013) also showed the importance of purge to feed ratio, adsorption pressure, feed flow rate, step times, and carbon ratio for layered two- and four-bed 6-step PSA processes for H2 recovery from coal gas. The result of the study is that higher purity of the product can be achieved with layered beds; however, less recovery can also be observed.

One of the main difficulties in mathematical adsorption modeling is the correct definition of adsorption thermodynamics and mass transfer. The EL (extended Langmuir) (Duong, 1998) isotherm is widely used due to the model's simplicity. However, the accuracy of this isotherm type is questionable. Even though it has a theoretical basis behind it, the assumptions place significant restrictions on the applicability of this isotherm. The EL model is an explicit model that is preferred over its implicit counterparts, for example, IAST (Ideal Adsorption Solution Theory), due to the computation complexity of the last one. An essential shortcoming of the EL model is the neglect of the adsorbate size effect (Tom et al., 2021). However, the results of studies that use EL are usually coherent with experimental data. In this study, more components will be considered, which may have a negative effect when a simple EL model is used.

The adsorption mass transfer model defines the mass accumulation in the solid phase. The most common is to use the LDF (Linear Driving Force) for estimating the mass transfer. Kim et al. (2015) indicate that the optimal parameters of mass transfer constants should be obtained by comparing

the numerical results with experimental data. These parameters should be chosen such that the model solution is the closest to the whole range of available experimental data.

Even though PSA systems are well known, the multicomponent VOC VPSA systems are not properly investigated. The VOC VPSA modeling is becoming critical to the industry as increasingly stringent emission standards are being set. In addition, modeling in python is more and more advantageous since it provides practical optimization tools.

1.1 The VPSA process

The VPSA process can be done in different ways (with two or more adsorbers, with three or more steps, and with co-current and counter-current flow configurations). The simplified flow diagram of VOC adsorption process studied in this work is shown in Fig. 1. The process consists of two beds: one in adsorption mode and another in regeneration mode. The adsorber outlet is a pure product during the adsorption process and highly concentrated vapor during the regeneration process. This vapor is then recycled in the absorption system.

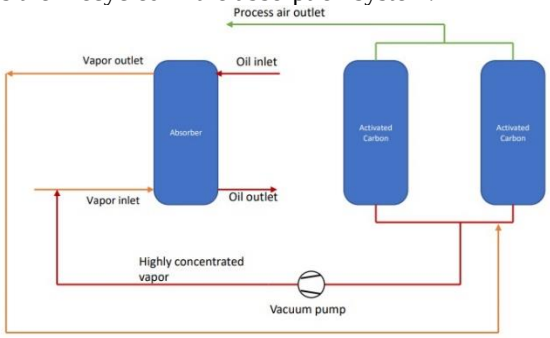

Figure 1: The simplified process flow diagram of VOC adsorption

One way of VPSA organization is co-current pressurization, adsorption, counter-current desorption, and counter-current purge. The steps are switched by employing valves. The top of the adsorber is closed during pressurization, and the system's pressure increases (see Fig. 2, upper left). The pressure increase occurs from a specific low pressure after regeneration to that required for adsorption. Next, the valve at the top of the adsorber opens, and the pure product is achieved at the outlet (see Fig. 2, upper right). After a certain period, the breakthrough of specific components occurs, and it is necessary to switch the adsorber to the regeneration mode (see Fig. 2, lower left). There is no inflow at the bottom during regeneration. Also, the valve to the vacuum pump opens, and the vacuum pump turns on. After some time, inert gas is supplied from the top while the pump operates. This step is called "purge" (see Fig. 2, lower right). As a result, the adsorbates' partial pressure decreases, which causes them to desorb better. After the purge, the whole cycle repeats. A certain amount of non-desorbed gas remains in the adsorber, which affects the process and changes the result of the next cycle. However, the system gradually converges with an increase in number of cycles to the so-called "cyclic-steady-state".

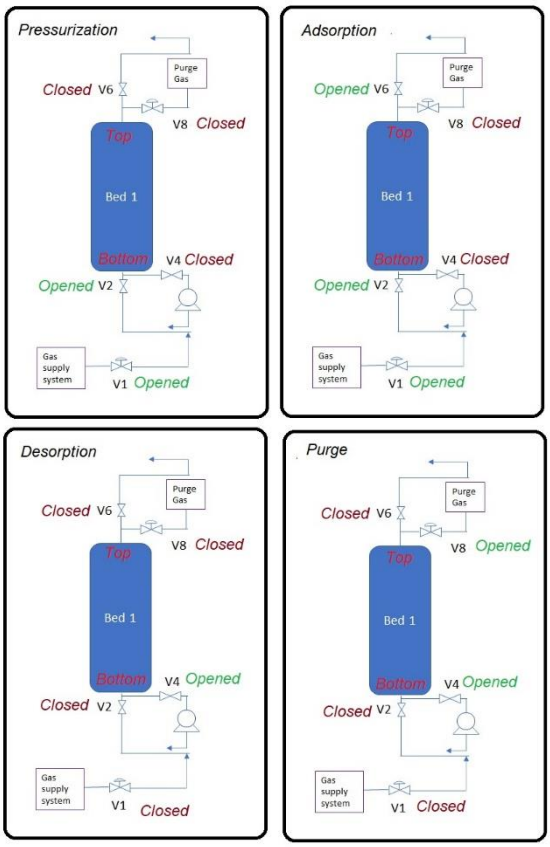

Figure 2: Cycle organization

1.2 Adsorption Equilibrium and Mass transfer

The extended Langmuir (EL) isotherm is widely used to describe the adsorption equilibrium due to the model's simplicity (see Eq. (1)).

$$\frac{w_{eq,i}}{w_{max,i}} = \frac{b_i P_i}{1 + \sum_{j=1}^{N} b_j P_j} \qquad (1)$$

here, $w_{eq,i}$ is an equilibrium concentration of the adsorbate in the solid phase [*kmol/kg*], $w_{max,i}$ is the maximum adsorbate concentration in the solid phase [*kmol/kg*], b_i is an affinity coefficient of component i [*1/bar*], P_i is a partial pressure of component *i* [*bar*], *N* - number of components, b_j is an affinity coefficient of component j [*1/bar*], P_j is a partial pressure of component j [*bar*].

Coefficient b is the parameter that shows the ratio between adsorption and desorption rates. This parameter is called affinity coefficient and may be expressed in terms of adsorption heat, temperature, and affinity constant:

$$b_i = b_\infty \, exp\left(\frac{Q}{RT}\right) \quad (2)$$

here, b_∞ is an affinity constant [*1/bar*], Q is an isosteric heat of adsorption [*J/mol*], R is a universal gas constant R = 8.314 [*J/molK*], T is temperature [*K*].

The IAST is widely used to describe multicomponent adsorption. One of the challenges in the theory is that it requires the evaluation of the spreading pressure, which is not available in the analytical form for many isotherms. However, any isotherm that can express spreading pressure analytically can be used in Fast IAST (Fast Ideal Adsorption Solution Theory), such as one-component Langmuir isotherm. The calculation procedure is described in more detail by Duong (1998).

The mass transfer resistance between gas and solid phases plays a great role in adsorption modeling. The mass transfer model defines the mass accumulation in the solid phase. The most common is to use the LDF model (see Eq. (3)) for estimating the mass transfer coefficient. The lumped mass transfer coefficient (overall mass transfer coefficient k_i in Eq. (3)) considers all the resistances to the mass transfer. They are the film around each particle, surface diffusion, macropore, and micropore diffusion in each particle.

The optimal mass transfer constants can be obtained from the comparison of the numerical results with experimental data.

$$\frac{\partial w_i}{\partial t} = \rho_{bulk} k_i (w_{eq,i} - w_i) \quad (3)$$

here, ρ_{bulk} is a solid bulk density [*kg/m3*], k_i is an overall mass transfer coefficient of a component i [*1/s*].

1.4 Governing transport equations

The transport equations include mass, momentum, and energy balance equations. The following assumptions are used:

1. Bed porosity is homogeneous and constant along the bed.
2. Gas flows only in axial direction and there are no gradients in radial direction (one-dimensional model).
4. Diffusion in axial direction are negligible.
5. Ideal gas law is used for gas state calculations.
6. Solid thermal conductivity is negligible and heat capacity is assumed to be constant and independent of temperature.
7. Gas thermal conductivity is negligible and heat capacity is assumed to be constant (independent of temperature and gas composition).
8. There is no thermal resistance between gas and solid phase.
9. The heat of adsorption is assumed to be constant, independent of loading and temperature.
10. Constant wall temperature assumption. Wall temperature is equal to the ambient temperature.

The mass balance equation:

$$\frac{10^2 \epsilon}{RT}\frac{\partial (y_i P)}{\partial t} - \left(\frac{10^2}{RT}\right)\left(\frac{B}{\mu}\right)\left(y_i P \frac{\partial^2 P}{\partial x^2} + y_i \left(\frac{\partial P}{\partial x}\right)^2 P \frac{\partial P}{\partial x}\frac{\partial y_i}{\partial x}\right) + \frac{\partial w_i}{\partial t} = 0 \quad (4)$$

here, ϵ is a total porosity, R is a universal gas constant [*J/kmolK*], T is temperature [K], B is bed permeability [m^2], μ is a dynamic gas viscosity [$bar\ s$], P is pressure [bar], y_i is a molar fraction of component i, w_i is a solid loading [$kmol/m^3$].

The energy equation:

$$\left(c_{p,solid}\rho_{bulk} + \epsilon c_{p,gas}\left(\frac{P \cdot 10^2}{RT}\right)\right)\frac{\partial T}{\partial t} - c_{p,gas}\left(\frac{P \cdot 10^2}{RT}\right)\left(\frac{B}{\mu}\right)\left(\frac{\partial P}{\partial x}\frac{\partial T}{\partial x}\right) = \frac{4h_W}{d}(T_{amb} - T) + \sum_{i=1}^{N}\frac{\partial w_i}{\partial t}\Delta H_i \quad (6)$$

here, $c_{p,solid}$ is a solid specific heat capacity [*J/kgK*], $c_{p,gas}$ is a gas specific heat capacity [*J/kmolK*], h_W is a wall heat transfer coefficient [W/m^2K], d is a diameter of the adsorber [m], T_{amb} is an ambient temperature [K], ΔH_i is a heat of adsorption of component i [*J/kmol*].

1.5 Boundary and initial conditions

The prescribed equations are subject to boundary and initial conditions:

Table 1: Boundary and initial conditions for pressurization and adsorption steps.

Pressurization	Adsorption
$P(x, t = 0) = P_{initial}$	$P(x, t = 0) = P_{press}$
$P(x = 0, t) = P_1(t)$	$P(x = 0, t) = P_{inlet}$
$P(x = L, t) = P_2(t)$	$\frac{\partial^2 P}{\partial x^2}(x = L, t) = 0$
$y_i(x = 0, t) = y_{i,feed}$	$y_i(x = 0, t) = y_{i,feed}$
$T(x, t = 0) = T_{initial}$	$T(x, t = 0) = T_{press}$
$T(x = 0, t) = T_{inlet}$	$T(x = 0, t) = T_{inlet}$

Table 2: Boundary and initial conditions for desorption and purge steps.

Desorption	Purge
$\mathrm{P(x,t=0)} = P_{ads}$	
$\mathrm{P(x=0,t)} = P_1(t)$	$\mathrm{P(x,t=0)} = P_{des}$
$\mathrm{P(x=L,t)} = P_2(t)$	$\mathrm{P(x=0,t)} = P_1(t)$
$\frac{\partial y_i}{\partial x}(\mathrm{x=L,t}) = 0$	$\mathrm{P(x=L,t)} = P_2(t)$
	$y_{N2}(\mathrm{x=L,t}) = 1$
$\mathrm{T(x,t=0)} = T_{ads}$	$\mathrm{T(x,t=0)} = T_{des}$
$\frac{\partial T}{\partial x}(\mathrm{x=L,t}) = 0$	$T(\mathrm{x=L,t}) = T_{inlet}$

here, $P_{initial}$ is the initial pressure along the adsorber for the first cycle or pressure along the adsorber after purge step for the next cycles $[bar]$, $P_1(t)$ is the pressure at the bottom (inlet) of the adsorber $[bar]$, $P_2(t)$ is the pressure at the top (outlet) of the adsorber $[bar]$, $y_{i,feed}$ is the molar fraction of component i in the feed stream, $T_{initial}$ is the initial temperature along the adsorber for the first cycle or temperature along the adsorber after purge step for the next cycles $[K]$, T_{inlet} is the gas inlet temperature $[K]$, subscripts *press, ads, des* mean the results of temperature or pressure from the previous step.

P1(t) and P2(t) are the boundary pressures at the bed bottom (inlet) and top (outlet) respectively. These pressures are calculated based on the ideal gas law using the following equations:

1. Pressurization

$$\frac{\partial P_1}{\partial t} = \frac{P_1}{V_1}\left(\frac{FRT \cdot 10^{-2}}{P_1} - u_{out}A\right) \quad (7)$$

$$\frac{\partial P_2}{\partial t} = \frac{P_2}{V_2}(u_{in}A) \quad (8)$$

2. Desorption

$$\frac{\partial P_1}{\partial t} = \frac{P_1}{V_1}(-q_{pump} - u_{in}A) \quad (9)$$

$$\frac{\partial P_2}{\partial t} = \frac{P_2}{V_2}(u_{out}A) \quad (10)$$

3. Purge

$$\frac{\partial P_1}{\partial t} = \frac{P_1}{V_1}(-q_{pump} - u_{in}A) \quad (11)$$

$$\frac{\partial P_2}{\partial t} = \frac{P_2}{V_2}(q_{purge} + u_{out}A) \quad (12)$$

here, F is the flow rate coming into the adsorber $[kmol/s]$, V_1 is an inlet volume not filled with adsorbent $[m^3]$, V_2 is an outlet volume not filled with adsorbent $[m^3]$, u_{out} is a velocity of gas going to the adsorber $[m/s]$, u_{in} is a velocity of gas going out of the adsorber $[m/s]$, q_{pump} is a volumetric flow rate to the vacuum pump $[\mathrm{m^3/s}]$, q_{purge} is a purge volumetruc flow rate to the adsorber $[\mathrm{m^3/s}]$.
It should be noted that velocity has a negative sign during desorption and purge steps.

2. Methodology

2.1 Python numerical solution

The set of PDEs (Partial Differential Equations) and ODEs (Ordinary Differential Equations) need to be solved with the initial and boundary conditions as shown in Tables 1 and 2.

The spatial and time derivative terms can be approximated. The variables are defined on a grid with finite difference methods.

The first-order upwind difference scheme may be beneficial in the case of sharp front propagation, which is vital in the simulation beginning and in the systems where breakthrough curves are steep. The first-order upwind method is also recommended because of the fast simulation. The scheme is first-order accurate and may give a significant numerical diffusion. However, the method does not produce oscillations (unconditionally stable). The upwind difference scheme for the positive velocity is shown below:

$$\frac{\partial f}{\partial x} = \frac{f_l - f_{l-1}}{\Delta x} \; if \; u > 0,$$

$$\frac{\partial f}{\partial x} = \frac{f_{l+1} - f_l}{\Delta x} \; if \; u < 0 \quad (13)$$

here, f is a function, l is a space grid point, u is velocity.
The second order derivative approximation is shown below:

$$\frac{\partial^2 f}{\partial x^2} = \frac{f_{l+1} - 2f_l + f_{l-1}}{\Delta x^2} \quad (14)$$

The system of PDE and ODE will be solved in Python.

2.2 Aspen Adsorption numerical solution

Aspen Adsorption will be used to compare the results. Aspen Adsorption is a comprehensive flowsheet simulator for adsorption modeling. The developed flowsheet with one adsorber for VPSA process is shown in Fig. 3.

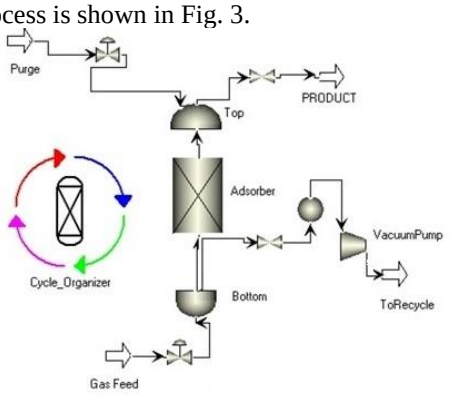

Figure 3: Aspen Adsorption VPSA flowsheet

3. Results

3.1 Model verification

3.1.1 Comparison with Cavenati et al. (2005) experiments

The simulation becomes more complicated with an increase in the number of components. Therefore, it is better first to compare the results with fewer components to investigate if the simulation works correctly. For example, Cavenati et al. (2005) considered only two components' adsorption on AC molecular sieve 3K: methane and carbon dioxide.

Cavenati et al. (2005) focused on vacuum pressure swing adsorption for the separation of methane (55 mol %) - carbon dioxide (45 mol %) mixture with a total flow between 1 and 1.5 SLPM (Standard Liter per Minute). A four-step cycle consisted of pressurization, adsorption, counter-current blowdown, and counter-current purge. The results for binary methane-carbon dioxide adsorption at a constant pressure of 320 kPa are presented. The authors did the experiments in a column of 0.83 m length and 0.021 m in diameter with a bulk density of 715 kg/m^3 . The ambient temperature during the experiments was 303 K.

Equilibrium and kinetic parameters for methane-carbon dioxide mixture adsorption on Carbon Molecular Sieve 3K can be found in Vilardi's work (Vilardi et al. 2020).

Fig. 4 shows the simulated breakthrough curves and experimental results for non-isothermal conditions. The model describes well the trend of breakthrough for methane and carbon dioxide.

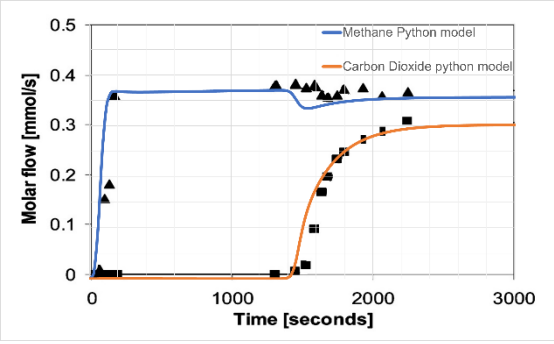

Figure 4: Comparison of breakthrough results with experiments (experimental results from Cavenati et al. (2005))

An essential part of the simulation is energy balance. Carbon dioxide adsorption produces a significant amount of heat. Cavenati et al. (2005) also reported a substantial amount of heat loss to the environment that needs to be considered. Therefore, wall heat transfer coefficient of 4E-5 MW/m^2K was used as a fitting parameter, and the result is shown in Fig. 5. The experimental data includes temperature profiles at three positions of the adsorption bed (0.17, 0.43, and 0.68 m). These temperature profiles were compared with simulated ones.

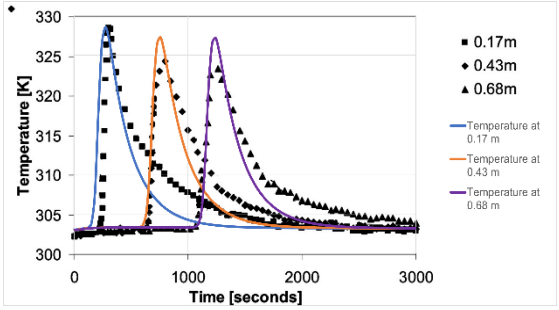

Figure 5: Comparison of temperature results with experiments (experimental results from Cavenati et al. (2005))

The results reflect the thermal wave well, but temperature profiles are more sharp than experimental. That may be due to the inaccuracy of the component properties (such as the heat capacity of gas and adsorbent) and neglection of axial thermal conductivities.

Next, Cavenati et al. (2005) presented the results after 46 cycles for VPSA system. The results of the experiments as well as the developed python simulation results are shown in Fig. 6. During the first 80 seconds of a cycle, the pressure rises from 10 kPa to 320 kPa with the constant feed flow rate of gas (see Fig. 2, upper left). The outlet flow rate of methane and carbon dioxide is 0 during this step because the top of the column is closed. During the next 100 seconds, the top of the column is opened, and the adsorption step with constant pressure and inlet flow rate begins (see Fig. 2, upper right). Only methane is obtained as the product at this step. From 180 to 300 seconds, the top of the column is closed, and counter-current blowdown occurs with the vacuum pump (see Fig. 2, lower left). The characteristic of the MZ 1C vacuum pump was used in the developed model. The final desorption pressure of 10 kPa coincides with what the authors presented in the article. In the next 50 seconds, there is a counter-current purge to decrease the partial pressure of carbon dioxide inside the adsorber (see Fig. 2, lower right).

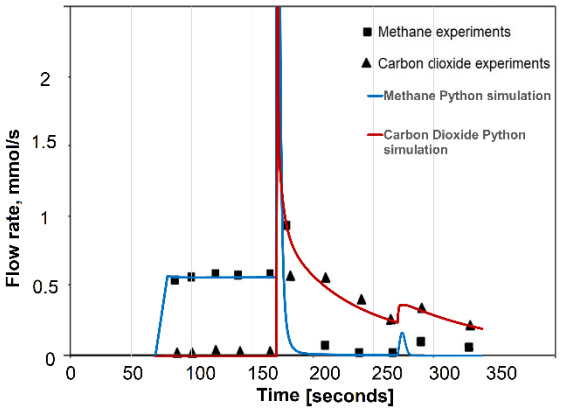

Figure 6: Comparison of temperature results with experiments (experiment results from (Cavenati et al., 2005))

3.1.2 VOC simulation and comparison with Aspen Adsorption results and Equinor experiments

The central part of the study deals with simulation of VOC adsorption on AC. The experiments were conducted at Equinor to optimize the adsorption of VOC on AC adsorption bed (Eroshkin, 2022). Adsorber design, cycle details and operating conditions are described in Tables 3-5. The adsorption cycle in the experiments was as described in Section 1.1 (see Figure 2):

Table 3: Bed parameters

Parameter	Value
Adsorber height	1 m
Adsorber height (filled with AC)	0.77 m
Adsorber diameter	0.032 m
Clean adsorbent bulk density	430 kg/m^3

Table 4: Cycle steps

Cycle step	Time
Pressurization	Until 1 bara is reached
Adsorption	900 sec/1500 sec
Desorption	600 sec / 1200 sec
Purge	300 sec

Table 5: Parameters of the main case study

Parameter	Value
Gas inlet flow rate	1248/1254 Nml/min
Purge gas flow rate	50 Nml/min
Composition	CH_4: 8.6 / 8 mol% C_2H_6:16.1 / 16 mol% C_3H_8: 22.4 / 20.4 mol% C_4H_{10}: 10 / 11.7 mol% CO_2 : 4.7 / 4.6 mol%, N_2: 38.2 / 39.3 mol%
Inlet temperature	303 K
Adsorbent initial temperature	303 K

Since the temperature variations do not exceed 10 degrees in the experimental results of VOC adsorption, neglecting temperature calculations should not radically change the solution. Thus, the isothermal simulation is presented below. The main parameters fitting to the model are the mass transfer coefficients. The mass transfer coefficients are initially assumed to be high, and there is almost no adsorption resistance.
The following parameters are used for equilibrium description. However, these parameters still need to be improved with proper experiments.

Table 6: Equilibrium parameters

Methane	Ethane
w_{max}: *0.00032* $\frac{kmol}{kg}$ b: 0.65 bar^{-1}	w_{max}: 0.0008 $\frac{kmol}{kg}$ *b: 3.06* bar^{-1}
Propane	**Butane**
w_{max}: *0.0018* $\frac{kmol}{kg}$ b: 3.8 bar^{-1}	w_{max}: 0.0018 $\frac{kmol}{kg}$ *b: 8* bar^{-1}
Carbon Dioxide	**Nitrogen**
w_{max}: *0.00075* $\frac{kmol}{kg}$ b: 0.73 bar^{-1}	w_{max}: 0 $\frac{kmol}{kg}$ *b: 0* bar^{-1}

Fig. 7 shows the change in pressure for the first case (15 min cycle and 1248 Nml/min inlet flow rate). When the pressure reaches just above 1 bar, the adsorption process begins while the pressure remains constant. The adsorption cycle lasts 15 minutes, after which the vacuum pump is turned on, and the pressure reduces rapidly to 0.06 bar during 300 seconds of regeneration. Then pressure rises slightly after desorption due to the desorption of heavy hydrocarbons (HC) with the purge. The model developed in Aspen Adsorption (see Fig. 3) shows approximately the same pressure result as the model developed in Python.

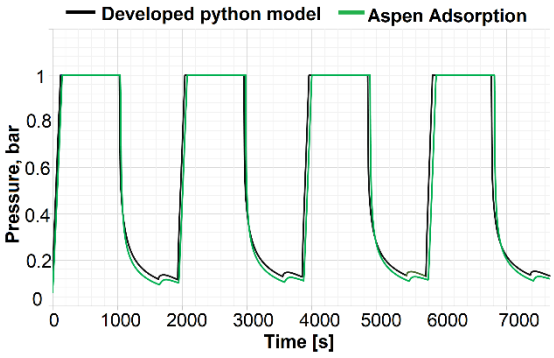

Figure 7: Pressure development during VPSA cycles

The graphs shown in Figs. 8 represent the molar flow rate of each gas exiting the adsorber after 10 simulated cycles. Cycle 1 means that all four stages were carried out only once: pressurization, adsorption, desorption, and purge. Thus, the number of cycles means how many times this 4-step cycle was simulated, using the final state from the previous cycle as the initial condition for the next cycle. Initially, the adsorber is assumed to be in equilibrium with nitrogen at 0.06 bar. However, some other adsorbed components remain adsorbed after the first cycle, affecting the next cycle. When the differences between cycles begin to be less than 1%, one can argue that the system has come to the so-called cyclic-steady-state.

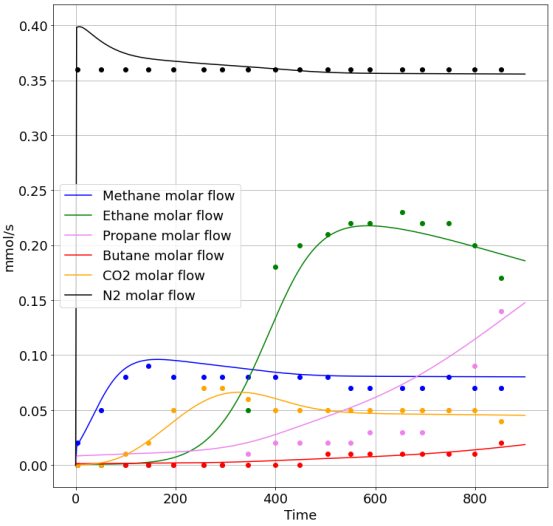

Figure 8: Comparison of the experimental and simulated results of VOC adsorption on AC with 15 min cycle and inlet flow rate 1248 Nml/min

Figures 9, and 10 show the capture efficiency when the cyclic-steady-state is reached for the cases with 15 min cycle and 25 min cycle. Capture efficiency of 100 % means no flow rate of a component exiting the column. Capture efficiency of 0 % means that the outlet molar flow rate of a component is equal to the inlet molar flow rate. The negative efficiency means that the outlet flow rate is higher than the inlet. As one can see from the model the capture of various VOC happens differently. The competitive behavior can be noticed. Once an equilibrium zone is formed in the AC, components with stronger affinity will push components with less affinity out of the adsorbent. Consequently, the outlet flow of "weak" components will increase above the inlet flow. It is seen from the graph that heavier components bind to the AC stronger than lighter components.

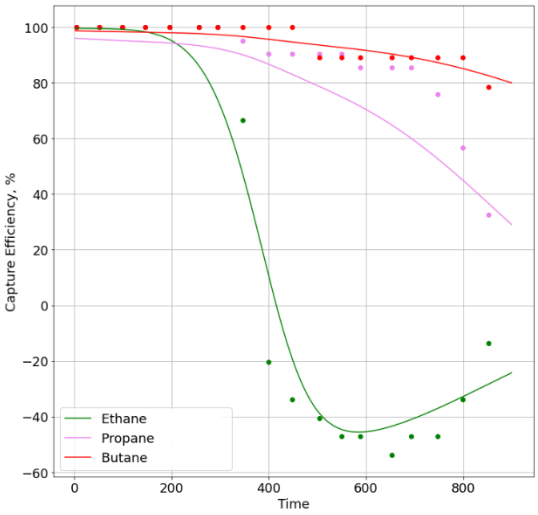

Figure 9: Capture efficiency. Molar flow 1248 Nml/min and cycle time 15 min

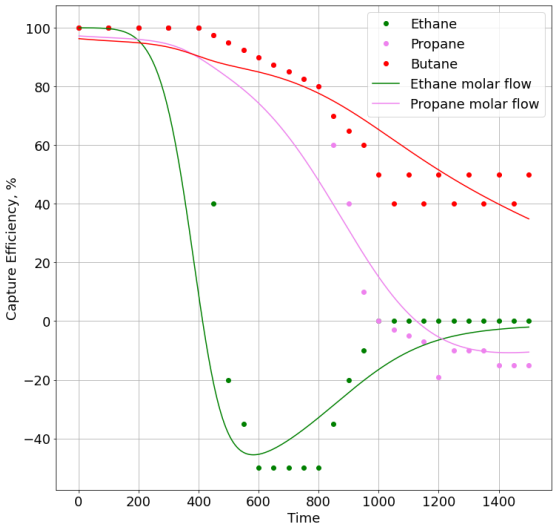

Figure 10: Capture efficiency. Molar flow 1254 Nml/min and cycle time 25 min

4. Summary and Discussion

The developed python model for VPSA simulation showed good agreement with Aspen Adsorption simulations, Cavenati et al. (2005) experiments and some multicomponent VOC experiments. It can be confirmed that the model calculates correctly; however, the equilibrium and kinetics parameters for the six-component mixture need to be improved. The available experimental data on equilibrium and kinetics is limited, and more accurate model predictions can be achieved by conducting more equilibrium and kinetic experiments.

5. Conclusion

The proper development of the adsorption process with high performance involves the design of a model that can describe the dynamic of adsorption, considering all relevant transport phenomena. The developed model in python can be used for prediction and theorical description of competitive VOC adsorption. The multicomponent adsorption isotherm and LDF equation for mass transfer reasonably well predict the adsorption behavior of 2 component VOC mixture (methane and carbon dioxide). When it comes to the six-component mixture, some adjustment required to get a good comparison with experimental data.

References

Ahn, S. et al. (2013) 'Layered two- and four bed PSA processes for H2 recovery from coal gas', *Chemical Engineering Science*, pp. 413–423. doi:10.1016/j.ces.2011.09.053

Cavenati, S. et al. (2005) 'Upgrade of methane from Landfill gas by pressure swing adsorption', Energy and Fuels, pp. 5108–5117.

Duong, D. (1998) 'Adsorption Analysis: Equilibria and Kinetics'. *Imperial College Press*. Vol. 2, 11

Eroshkin, S (2022) 'Volatile Organic Components Adsorption on Activated Carbon'. Master's Thesis. Norwegian University of Science and Technology.

Esteves, I. et al. (2003). 'Adsorption of Natural Gas Components on Activated Carbon for Gas Storage Applications'. C-H. Lee (Ed.), *Proceedings of the Third Pacific Basin Conference on Adsorption Science and Technology* (pp. 479-483). World Scientific Publishing Co. Pte Ltd. doi:10.1142/9789812704320_0086

Kim, Y.J. et al. (2015). 'Study on a numerical model and PSA (pressure swing adsorption) process experiment for CH4/CO2 separation from biogas', *Energy (2015)*, pp. 732–741. doi:10.1016/j.energy.2015.08.086.

P.Cruz et al. (2003) 'Cyclic adsorption separation processes: analysis strategy and optimization procedure', Chemical Engineering Science 58, pp. 3143–315. doi:10.1016/S0009-2509(03)00189-1

Shuangjun, L. et al. (2018). 'Mathematical modeling and numerical investigation of carbon capture by adsorption: Literature review and case study'. *Applied Energy 221*, pp. 437–449.

Tefera, D.T. et al. (2014) 'Modeling competitive adsorption of mixtures of volatile organic compounds in a fixed-bed of beaded activated carbon', Environ Sci Technol. 48(9), pp. 5108-17. doi: 10.1021/es404667f. Epub 2014 Apr 8. PMID: 24670053.

Tom, R. C. et al. (2021) 'Adsorption Size Effects for Langmuir Systems in Process Simulators: Case Study Comparing Explicit Langmuir-Based Models and FASTIAS' , *Industrial & Engineering Chemistry Research 60* (32), pp. 12092-12099. doi: 10.1021/acs.iecr.1c01657.

Vacuum pump VacuuBrand MZ1C. url: https://shop.vacuubrand.com/en/chemistry-diaphragm-pump-mz-1c-20724100.html#description

Vilardi, G. et al. (2020). 'Exergy and energy analysis of biogas upgrading by pressure swing adsorption: Dynamic analysis of the process', Energy Conversion and Management 226. doi: 10.1016/j.enconman.2020.113482.